# Thermodynamic study of adsorption of nickel ions onto carbon aerogels

Rafael A. Fonseca-Correa [a], Liliana Giraldo [b], Juan Carlos Moreno-Piraján [a],*

[a] Facultad de Ciencias, Departamento de Química, Grupo de investigación en Sólidos Porosos y Calorimetría, Universidad de los Andes, Bogotá, Colombia
[b] Facultad de Ciencias, Departamento de Química, Universidad Nacional de Colombia, Bogotá, Colombia

## ABSTRACT

In this work, 8 samples of carbon aerogels with different ratios of catalyst versus resorcinol (R/C) from 25 to 1500 were used. The textural properties were evaluated from $N_2$ adsorption isotherms in 77 K, as well as the chemical ones, where the surface chemistry was evaluated through the Boehm titrations. The results were analyzed and related to the adsorption of the nickel (II) ion from aqueous solution. The experimental results show that the aerogel samples can be divided into two series with different properties: Series I, mainly microporous (low ratio R/C) and Series II (high ratio R/C) mainly microporous but with a contribution of mesoporosity. The specific surface area varied between 64 and 990 m$^2$ g$^{-1}$. The experimental results show that prepared aerogels have an adequate adsorption capacity towards nickel (II) ions. The behavior of the kinetics of Ni(II) adsorption on carbon aerogels adjusts in a better way the kinetic model of pseudo-second order since it is the one that presents the value of the highest R$^2$ correlation coefficient. The calorimetric data shows that the greater the area developed in carbons aerogels the enthalpy increases.

## 1. Introduction

The so-called bad industrial development has generated large disasters in ecosystems in recent decades, to the point that it has endangered lakes and rivers and indeed the life that exists in them. Additionally, the soils have become contaminated due to the poor disposal and/or treatment of the waste produced in the companies. Among these wastes sent to the environment (especially to aqueous systems) are the heavy metal ions. It is well documented in the scientific literature that the ingestion of metal ions causes serious problems to living beings. Among the metal ions that are highly toxic to life and ecosystems are chromium (Cr), copper (Cu), lead (Pb), mercury (Hg), manganese (Mn), cadmium (Cd), nickel (Ni), zinc (Zn) and iron (Fe), etc. This fact has led to research centers to raise research that generates new knowledge and produce solutions to this problem, due to the proven impact that this fact has on the health of the population, especially the less favored, who tend to feed on fish and agricultural products without any quality control. These foods and particularly marine animals are usually contaminated by absorption of various metals taken from wastewater as well as agricultural products, directly affecting the food chain where humans are involved, generating (as mentioned before) a high risk to the health of consumers. This wastewater comes from various industries, including metallurgy, tannery, chemistry, mining, etc. Which

within their processes use one or more of these heavy metals whose toxicity is high. These industries tend to throw into the environment some of these metals exceeding the levels allowed by the control entities of each country to the lakes, rivers and their effluents. Therefore, it becomes necessary to remove these heavy metals from wastewater by appropriate treatment before releasing them into the environment and/ or failing to pose a solution is when they are already in the ecosystems. One of these ions, which is worth mentioning because this research is the object, is the Ni(II) ion, which is classified as a micronutrient for plants, animals and humans. However, it is toxic in high concentrations. For example, exposure to nickel ion can cause skin allergies, pulmonary fibrosis, cancer of the respiratory tract [1, 2, 3], bone problems, dermatitis in the skin (itching of Ni) which is the most frequent effect of exposure to Ni, such as coins and jewelry.

Additionally, acute Ni(II) poisoning causes headache, dizziness, nausea and vomiting, chest pain, tightness in the chest, dry cough and shortness of breath, rapid breathing, cyanosis and extreme weakness [3, 4]. Additionally, heavy metal ions do not degrade, remain in the environment and tend to accumulate in living organisms. Considering its toxicity, the treatment of sewage contaminated with these metals continues to be a priority concern [3, 4]. Due to this, the development of materials for water purification at a domestic and industrial level is still current and important. Some of the most commonly used methodologies

---

* Corresponding author.
*E-mail address:* jumoreno@uniandes.edu.co (J.C. Moreno-Piraján).

in the treatment of wastewater include coagulation, flocculation, precipitation, sedimentation or filtration, membrane processes, ion exchange and adsorption using activated carbon (AC) [4, 5, 6, 7, 8]. However, the cost of these methods hinders their application as reported in the literature [9, 10]. In addition, at low concentration (1–100 mg/L) many of these treatments are quite inefficient in terms of cost [11]. Activated carbons have been used with very good effect in the treatment of aqueous solutions that contain a low concentration of metal ions [12, 13, 14, 15, 16]. Due to its large number of micropores and mesopores, its large surface [17], the variety of surface functional groups that interact with heavy metal ions and even the possibility of increasing adsorption capacity by modifying with other functional groups or with the use of additives [12, 13, 14, 15, 16, 17, 18, 19], these adsorbents are interesting candidates for wastewater treatment. Agro-waste has also received much attention as an economic source for the production of activated carbons. With these latter materials their cost-effectiveness makes them attractive particularly for small-scale industries [18, 19, 20, 21, 22]. Another type of interesting materials are the carbon aerogels have been materials that have emerged for a few decades and have been applied primarily in the storage of gases. However, due to the control that can be exercised during the synthesis, they can become a material that can be explored to retain contaminants from the aqueous phase. There are not many reports in the scientific literature about the use of this type of materials in the retention of ions from aqueous solution. According to the above the scope of this research is to prepare carbon resorcinol/formaldehyde aerogels (R/F) in basic medium at different resorcinol/catalyst (R/C) ratios to explore the feasibility of using these materials for ion removal Ni(II) from aqueous solutions carrying out a study of the effect of pH, applying thermodynamic models to analyze which is adjusted and a detailed kinetic study. Calorimetric studies were carried out to evaluate the concordance of the results obtained.

## 2. Materials and methods

### 2.1. Adsorbents

#### 2.1.1. Preparation of carbon aerogels

The gels are prepared by the procedure already described in the literature [20]. Once obtained, drying to supercritical conditions is used to synthesize aerogels. Finally, the aerogels are subjected to a carbonization process in an inert atmosphere to obtain carbon aerogels. Resorcinol-formaldehyde gels, were prepared using resorcinol (R) (98% purity), formaldehyde (F) (37% solution), $Na_2CO_3$ (99.9% purity), all of Aldrich ™ brand, and deionized water. Resorcinol (0.1120 mol) was dissolved in deionized water (W) at a constant established ratio (R/W (0.075)). Next, the catalyst $Na_2CO_3$ (C) was added in different proportions (R/C): 25, 50, 100, 200, 400, 600, 800 and 1500, which acts as a catalyst of the reaction (basic catalyst) for accelerating the dehydrogenation of resorcinol. The solutions of resorcinol (R/F = 0.5) and formaldehyde are mixed and stirred vigorously. The solutions are then placed in cylindrical glass molds with a lid (7 cm long x 1 cm internal diameter), and then subjected to a temperature program to achieve gelation and curing: 1 day at 25 °C, 2 days at 50 °C and 3 days at 70 °C. The solvent is then removed in the gels obtained using supercritical fluid equipment with $CO_2$ at 41 °C and 120 bar pressure. Once dried, the aerogels are charred in a tubular furnace (brand Carbolite™ CTZ/TZF) under a nitrogen atmosphere of 100 mL/min, at 2 °C/min up to 850 °C for 3 hours. The aerogels were prepared under the following conditions: molar ratio resorcinol/formaldehyde 0.5. Resorcinol/catalyst ratios, eight different ratios: 25, 50, 100. 200, 400, 600, 800 and 1500, to achieve a broad spectrum of concentration and thus determine the changes in the porous structure obtained and be able to study as the effect of the Catalyst acts on each of the porous materials and its effect on Ni(II) adsorption. The resorcinol/solvent molar ratio used is 0.5. They were labeled as: carbon aerogels. Ae25, Ae50, Ae100, Ae200, Ae400, Ae600, Ae800 and Ae1500 [23, 24].

### 2.2. Adsorbates

The solutions of the Ni(II) ions were prepared with Sigma Aldrich analytical grade reagents, using nickel with Ni $(NO_3)_2.3H_2O$ and using double distilled water. The range of concentrations that were used for the study is 50–500 mg.L$^{-1}$. The reading of the curves of adsorption, calibration, and solutions of the isotherms was carried out in an atomic absorption spectrophotometer "Perkin Elmer, ANALYST 300".

### 2.3. Textural characterization. Adsorption isotherms $N_2$ at 77 K

The $N_2$ has a molecular dimension of 0.36 nm in kinetic diameter, [21]. In this way, an analysis of the $N_2$ adsorption isotherms at -196 °C provides an important set of data that allows us to fully understand the textural characteristics of the solids under study. In order to analyze the porous texture of the carbon materials obtained in this work, $N_2$ adsorption-desorption isotherms were made at -196 °C. The carbonaceous samples, of around 0.100 g, are previously degassed at 250 °C for a period of 3 h, in an IQ2 equipment, Quantachrome Co (Boynton Beach, FL, USA).

#### 2.3.1. Functional groups

##### 2.3.1.1. Boehm qualifications. The acid groups present in carbon materials are usually of the carboxyl, hydroxyl, phenol and lactone type, while the basic groups are of the pyrone, quinone and chromene type. The basicity of carbon material may also be due to the delocalization of electrons from the basal plane [22, 25, 26, 27]. To determine the quantity and type of oxygenated functional groups located on the surface of the studied materials, samples of these were submerged in different solutions of concentration 0.1 M as follows: The most used bases are NaHCO$_3$ (pKa = 6.37), $Na_2CO_3$ (pKa = 10.25), NaOH (pKa = 15.74), $C_2H_5ONa$ (pKa = 20.58) [3]. According to Boehm, the carboxylic groups are valued by NaHCO$_3$, the difference between the acidity valued by NaHCO$_3$ and $Na_2CO_3$ corresponds to the content of lactones, the phenolic groups are obtained by the difference between the registered acidity with NaOH and $Na_2CO_3$, and the Carbonyl groups are valued by sodium ethoxide. Finally, the hydrochloric acid gives an estimate of the total basicity of the material [21]. Approximately 0.1 gram of the adsorbent is immersed in 25 mL of the solution; the solutions are left at 25 °C, left in constant agitation for 5 days; Occasionally $N_2$ is bubbled over the solutions in order to remove the atmospheric $CO_2$, finally aliquots of 10.0 mL of the previously standardized solutions with acid or base are titrated and the mili-equivalent gram by difference is determined.

##### 2.3.1.2. Zero load point $pH_{pcc}$. The electro-kinetic properties of solids are a direct consequence of the surface chemical environment. In this way, depending on the surface chemistry of the solid, the material when placed in aqueous dispersion may present a specific surface charge at the interface, which may be an average negative, positive or neutral. It is known as pH at the point of zero charges ($pH_{pcc}$) at the pH value at which the number of positive charges is equal to that of negative charges, such that the net charge on the surface is zero. The tendency of the surface to be negatively or positively charged is thus measured. The carbon materials are characterized by having an amphoteric nature, which means that on the surface of the material surface acidic groups and surface groups of basic character coexist. In general: if the pH of the medium is greater than the point of zero charge of the carbonaceous material we will have a predominance of negative charges on the surface of the carbon material; on the other hand, if the pH of the medium is lower than the point of zero charge of the material, a positively charged surface will be obtained. To determine the pH at the point of zero load, quantities of the materials are weighed in a range of 0.050–0.300 g, placed in a 50 mL glass bottle and added with 10 mL of sodium chloride solution, NaCl 0.1 N. The bottles are covered and left in agitation at a constant temperature of 25 °C for 48

hours, then the pH of each of the solutions is measured. The zero charge point is determined as the pH at which the pH curve tends as a function of the mass of the sample in the suspension [22, 25, 26].

### 2.3.2. Immersion calorimetry

There are two large families of calorimeters: adiabatic and diathermic, which in turn are divided into "passive" and "active". Passive calorimeters are based on the conductivity or isolation of their materials, while active calorimeters make use of electronic temperature control or power compensation to achieve their adiabatic or diathermic character [27]. The calorimeter used in this work is classified as a passive diathermic calorimeter, microcalorimeter type of heat flow, in which thermal conduction is favored by a small thermal resistance which allows the flow of heat between the cell and the surroundings, this flow Detected by sensors. The sensor system consists of a thermopile. This type of sensors is governed by the Seebeck Effect, a thermoelectric property discovered in 1821 by the German physicist Thomas Johann Seebeck. In this effect, the temperature difference between two metallic or semiconductor materials induces an electrical potential [28, 29]. In an immersion calorimeter, the heat flow is presented by a small temperature difference between the surroundings and the cell, product of the immersion of the solid. The magnitude of the temperature difference depends on the amount of heat released per unit of time, the thermal conductivity, the geometry of the cell, the type of sensors and the thermal insulators of the calorimeter. The calorimetric experiments were carried out using a Calvet-type heat conduction calorimeter of local construction, the equipment uses thermal sensors thermopiles of semiconductor materials and, as a heat reservoir, an aluminum block in which a 10 mL stainless steel cell is inserted. of capacity in which 10 mL of the solvent is placed [30, 31]. To determine the immersion enthalpies, 0.100 g of the solid was weighed in a glass vial, then the vial was introduced into the stainless-steel calorimetric cell, where 10 ml of the selected immersion liquid is already available. And later it is assembled in the calorimeter inside the main heat reservoir. Under these conditions, the electric potential is captured until a baseline is obtained (this may require up to 2 h). Rupture of the fragile tip of the vial is made by slowly and gently pressing the vial down. This rupture produces a calorimetric effect of approximately 5 μV, which is not significant in the subsequent calculation of the enthalpy. The change in the potential signal, product of the immersion, is captured by the computational system until the base line is re-obtained (this usually requires approximately 30 minutes), finally the electrical calibration of the calorimeter is carried out. The experiments were repeated four times for each solvent mentioned above [30, 31, 32, 33, 34, 35].

### 2.3.3. Quantification of Ni(II) (by atomic absorption)

The reading of the calibration curves, adsorption of the isotherms and kinetics are made in an atomic absorption spectrophotometer "Perkin Elmer, ANALYST 300". To determine the effect of the pH of the solution on the adsorption capacity, 0.1 g of the solid is placed in 50 mL of 100 mg.L$^{-1}$ solution of the respective ion and the pH is adjusted to 2, 4, 6 and 8 with diluted solutions of 0.01 M NaOH and HNO$_3$. The solutions are thermostatted at 25 °C for the time necessary to achieve equilibrium. The solution is filtered to remove the solid and determine the concentration of the metals by atomic absorption. Prepare 6 solutions of known concentration (50–500 mg.L$^{-1}$), 50 mL of the solutions of the respective ion are placed in a 50 mL container. Then add 0.1 g of the solid to the solution and leave it under agitation and constant temperature, 25 °C, for the time necessary to reach equilibrium. The solution is filtered to remove the solid and the concentration of the metals is determined. by atomic absorption [36, 37, 38].

### 2.3.4. Adsorption kinetics

A solution of the respective ion is prepared at a concentration of 500 mg.L$^{-1}$. 1.0 g of the solid is placed in the solution at a constant temperature of 25 °C, and 2 mL aliquots are taken at different time intervals

for 4 consecutive days. Small sample volumes are taken (without the presence of aerogel in the suspension) for which a syringe is used, to which a 0.50-micron filter has been attached at the end [26, 27, 28, 29, 30, 31, 32, 33].

## 3. Results and discussion

### 3.1. Analysis synthesis aerogels of carbon

The color of the gels changes as the ratio R/C is modified. The samples have a color from brown to orange ending in light yellow, from lower to the higher ratio R/C. Table 1 shows the initial and final synthesis pHs. The pH was measured at the initial solution when the resorcinol and the catalyst, which is the sodium carbonate, were mixed before adding the formaldehyde and at the end of the mixture when all the formaldehyde was added, and the solution was allowed to stir for 30 minutes, before starting the curing or gelation process.

These pH variations are due to the structure that obtains, the monomeric units and the functional groups formed in the primary structure to later form the crystalline network [39, 40]. After the supercritical drying process, the aerogels darken becoming opaquer, the structure becomes more fragile and porous in appearance as the R/C ratio increases, but without losing the monolith structure.

In (Fig. 1), the moment in which the polymeric gel is introduced to the supercritical fluid equipment reactor is shown; it is observed that by designing the reactor it is possible to maintain the monolith type structure without having to fractionate the sample, this is an advantage for possible applications of aerogels as catalysts inside reactors or electrodes inside electrochemical cells [39, 40, 41, 42].

After supercritical drying, the gels are subjected to the pyrolysis process under a nitrogen atmosphere at 850 °C, at which time the proportion of carbon in the samples increases, to obtain the carbon aerogels. These structures are somewhat more fragile than dry gels, this is probably due to the breakage of existing links between carbon nodes and the lesser destruction of the structure due to the effect of stresses on the structure when removing the solvent under supercritical conditions. In Fig. 2, the characteristics for the aerogels Ae600 and Ae1500 are shown, both for the polymeric aerogel and for the carbon aerogel.

The shrinkage of the structure is observed after the pyrolysis process, the contraction of the structure is observed after the pyrolysis process, due to the series of reactions that end in this stage. In Table 2, the values for the elemental analysis in the whole series of carbon aerogels by EDS are shown. Hydrogen % is calculated by the difference between 100% and the Carbon and Oxygen content [43, 44]. The density values and the Burn-off obtained in the furnace pyrolysis process are also recorded.

The carbon content increases as the R/C ratio increases. The hydrogen content is slightly lower and the oxygen content is higher, suggesting that the formation of oxygen functions is further promoted. The density obtained is low, which suggests that important changes are already being induced by the drying method, where supercritical drying has high importance in the final structure of the obtained material [45], and also decreases with increasing R/C ratio. The burn-off takes values between 62.34% and 66.36%.

**Table 1**
Synthetic pH of the carbon gels.

| Sample | pHi | pHf |
|--------|------|------|
| Ae25 | 8.57 | 8.19 |
| Ae50 | 8.42 | 7.89 |
| Ae100 | 8.35 | 7.66 |
| Ae200 | 7.74 | 7.01 |
| Ae400 | 7.16 | 6.86 |
| Ae600 | 6.31 | 6.17 |
| Ae800 | 6.18 | 6.08 |
| Ae1500 | 5.58 | 5.27 |

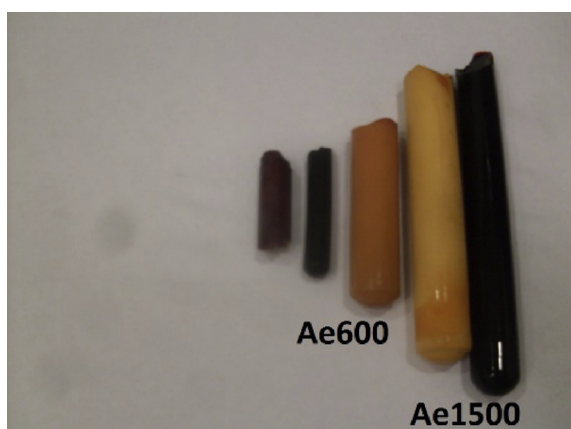**Fig. 1.** Polymeric gel when introduced to the supercritical drying reactor for sample Ae25 and Ae200.



**Fig. 2.** The appearance of polymer gels and carbon aerogels, for the samples: Ae600 and Ae1500.

## 3.2. Study of the acidity and basicity of aerogel

Table 3 shows the results obtained for the determination of the surface groups by the Boehm method and the determination of the pH at the point of zero charge ($pH_{pcc}$). The type and concentration of surface functional groups in carbon aerogels have been studied using methods of analysis such as Boehm titration, determination of the pH at the point of zero charge by mass titration.

The total acidity for the samples of carbon aerogels is greater than the total basicity. This may be due to the oxidation process undergone by the polymeric gel in the drying process with supercritical $CO_2$, which induces the formation of more acidic oxygenated functional groups than polymeric gels dried to subcritical conditions. The lactonic groups are in smaller proportion with respect to the carboxylic groups while the phenolic groups are present, in a low proportion in the samples Ae25, Ae200, Ae600, Ae800, and Ae1500. With respect to the number of acid surface groups, in each case, no specific trend is observed with respect to the R/C ratio. When the carboxylic, lactic and phenolic groups predominate, the surface of the carbonaceous structure presents good characteristics for the exchange of cationic ions [46]. The presence of these groups, although to a lesser extent, may be due to the stability of these groups at a higher temperature than the acid groups and to the presence of π electrons delocalized on the surface of the carbonaceous structure of the carbon aerogel [47, 48, 49, 50, 51, 52, 53, 54, 55, 56, 57]. For low $pH_{pcc}$ values, the adsorption of metal cations is favored when the pH of the medium is higher than the $pH_{pcc}$ since the surface charge on the carbon aerogel will be negatively charged having an affinity for exchanging positive charges of the cationic ions. Care must be taken not to exceed the pH of the medium above the pH of precipitation of the cation as hydroxide since the phenomenon of adsorption will not occur.

In Fig. 3, the variation of $pH_{pcc}$ with respect to the different resorcinol and R/C catalyst ratios is observed, where a clear trend is observed. When increasing the R/C ratio decreases the $pH_{pcc}$, the Ae600 sample has
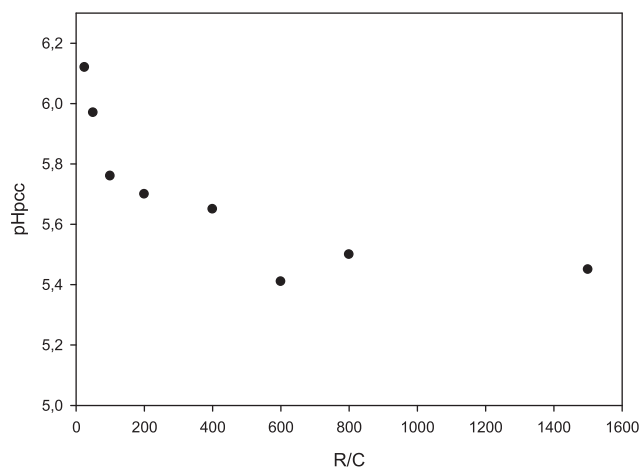


**Fig. 3.** Variation of $pH_{pcc}$ as a function of the change in the R/C ratio for carbon aerogels.

**Table 2**
Elemental analysis by EDS, density, and Burn-off for carbon aerogels.

| Sample | Analysis by EDS | | | Density | Burn-off |
| | C % | H % | O % | (g.cm$^{-1}$) | % |
|---|---|---|---|---|---|
| Ae25 | 90.45 | 1.98 | 7.57 | 0.772 | 62.34 |
| Ae50 | 90.34 | 1.87 | 7.79 | 0.885 | 64.78 |
| Ae100 | 90.97 | 1.44 | 7.59 | 0.749 | 65.82 |
| Ae200 | 91.25 | 1.24 | 7.51 | 0.705 | 64.45 |
| Ae400 | 91.57 | 1.12 | 7.31 | 0.672 | 66.02 |
| Ae600 | 91.83 | 1.03 | 7.14 | 0.644 | 66.63 |
| Ae800 | 92.09 | 0.98 | 6.93 | 0.632 | 63.17 |
| Ae1500 | 92.49 | 0.74 | 6.77 | 0.601 | 65.91 |

**Table 3**
Surface groups (mmol.g$^{-1}$) in carbon aerogels determined by Boehm titration and pH at the point of zero charge.

| GROUP | Lactonic | Carboxylic | Fenolic | Carbonyl | Total Acidity | Total Basicity | Total Groups | $pH_{pcc}$ |
| SAMPLE | mmol.g$^{-1}$ | mmol.g$^{-1}$ | mmol.g$^{-1}$ | mmol.g$^{-1}$ | mmol.g$^{-1}$ | mmol.g$^{-1}$ | mmol.g$^{-1}$ | |
|---|---|---|---|---|---|---|---|---|
| Ae25 | 0.885 | 2.111 | 0.045 | 0.000 | 3.041 | 0.825 | 3.865 | 6.12 |
| Ae50 | 0.936 | 2.133 | 0.000 | 0.000 | 3.069 | 0.491 | 3.560 | 5.97 |
| Ae100 | 0.828 | 1.905 | 0.000 | 0.000 | 2.733 | 0.502 | 3.235 | 5.76 |
| Ae200 | 0.902 | 2.064 | 0.042 | 0.000 | 3.009 | 0.975 | 3.984 | 5.70 |
| Ae400 | 0.946 | 2.255 | 0.000 | 0.000 | 3.200 | 0.961 | 4.161 | 5.65 |
| Ae600 | 0.940 | 2.829 | 0.044 | 0.000 | 3.813 | 0.864 | 4.677 | 5.41 |
| Ae800 | 0.921 | 2.229 | 0.043 | 0.000 | 3.193 | 1.065 | 4.258 | 5.50 |
| Ae1500 | 1.041 | 2.026 | 0.045 | 0.000 | 3.112 | 0.938 | 4.051 | 5.45 |

the lowest value of $pH_{pcc}$.

In carbon aerogels, being the $pH_{pcc}$ values are low and have a greater possibility of being negatively charged. There is a direct relationship between the classes of functional groups formed by the effect of the drying process in relation to the number of monomer units formed in the polymerization process. Because as the R/C ratio increases, the total groups tend to increase. Thus, finally, the distribution of the functional groups is due to the pyrolysis process, where the final structure of the carbon aerogel is formed with the oxidation of the samples when subjected to air.

### 3.3. Textural analysis of the different aerogels from the isotherms. of $N_2$

The textural characteristics of the carbon aerogels were determined by Adsorption isotherms of $N_2$ at 77 K. The use of models to determine the textural parameters in microporous solids is often displaced at lower pressures, as in the case of the linear range of the (Brunauer-Emmet and Teller) BET model, which is used for the calculation of apparent surface areas. The choice of relative pressure range relevant for the analysis of the apparent surface area with the BET model is of great importance due to the possibility of overestimating or underestimating the capacity of the monolayer, (the optimal range of P/P$^o$ is determined using the method proposed by Rouquerol and Col.) [30, 58]. For this model, it must be verified that for all the calculated areas the value of the constant C is positive (that is, any negative intersection in the graph B.E.T indicates that it is outside the valid range for the equation BET). The application of equation BET should be limited to the range where the term [V (1- P/P$^o$)] increases continuously with P/P$^o$ [23, 59, 60, 61, 62, 63, 64, 65]. The Dubinin-Astakhov model is used at P/P$^o$ <0.1, to perform the microporosity analysis, the Dubinin-Radushkevich model is applied in the range of P/P$^o$ <0.1. For the analysis of mesoporosity, model Barrett-Joyner-Halenda (BJH), (a P/P$^o$> 0.35–1, in the desorption branch) is used. The functional density theory is applied for pressures: P/P$^o$ = $10^{-6}$-1, the effect of different pore geometries is considered (cylinder, groove and combined cylinder-groove) and the effect of roughness, heterogeneity and homogeneity of the surface (QSDFT and NLDFT, respectively). The QSDFT model is used for the pore size distribution. For the study of all these models, the ASQiWin software is used. The detailed analysis of the results of the textural part have already been published in the literature by our research group [23, 24]. In summary, this interpretation concludes that the PSD (Pore Size Density) obtained from the adsorption of $N_2$ isotherms to 77 K using the kernel slot-cylinder pore modulation QSDFT (Quenched Solid Density Functional Theory) shows a micropore distribution in some cases monomodal and in other bi-modal. When compared with homologous data obtained by Immersion Calorimetry, the latter is adjusted with the PDS deduced by the QSDFT kernel assuming a cylindrical slot pore model for most samples, although it did not coincide exactly with some samples, due to limitations diffusion in the pore structure of the solid. The experimental results show that the aerogel samples can be divided into two series with different properties: Series I, mainly microporous (low ratio R/C) and Series II (high ratio R/C) mainly microporous but with a contribution of mesoporosity. The specific surface area varied between 64 and 990 m$^2$ g$^{-1}$ and the QSDFT model better equipped with a core with a porous cylinder system. The experimental results show a good concordance between the results obtained from immersion calorimetry in dichloromethane (instead of in benzene) and the corresponding obtained from the BET method applied to the $N_2$ adsorption isotherms [23].

Scanning electron microscopy (SEM) is normally used to study the topography of the sample. The maximum resolution of the SEM in the order of 3–5 nm, and the environment of the sample is normally vacuum. In the field of carbon materials, the SEM is usually used to study the topography of the sample, a detailed texture, the characteristics of the interface between different components in composite materials The micrographs obtained by scanning electron microscopy SEM, of the surface of the carbon aerogels at the same magnification to see the comparative

effects in relation to the structure changes.

The micrographs of carbon aerogels show, on a micrometric scale, the morphology of the external surface, which has cavities with a high degree of roughness, these spaces are of the order of 1 μm. Although the micropores and mesopores are not visible, the photographs show the shapes and location of the macropores on the surface of the sample. Macropores are formed during pyrolysis and the loss of volatile material and favor diffusional processes. It is evident that as the R/C ratio increases, the formation of structural aggregates increases. In the samples of the I-series, the structures are simpler with flat and sharp shapes where there is an incipient formation of interconnected structures. It is possible to deduce that the greater amount of catalyst plus monomer units are formed, resulting in the formation of some characteristics of the pearl necklace type for the samples of the series-II, proper for this type of materials. The micropores and mesopores evaluated by the textural analysis models are not evident in the micrographs of carbon aerogels. Some formations of cavities in the surface of the materials are observed and as the R/C ratio increases, there is an increase in the roughness of the samples without modifying the interconnected structure. The formation of the bonds between the carbons makes the connections between their nodules are intense, preventing the rupture of the networks that are formed as the R/C ratio increases [24]. Similarly, a good combination of pore size distribution data (PSD) obtained from isotherms of $N_2$ adsorption and immersion calorimetry was observed, except for a pair of aerogels. Finally, the experimental and modeling results were critically discussed in the aforementioned publication [23, 24].

### 3.4. Adsorption study of Ni(II) ion from the aqueous solution of carbon aerogels

#### 3.4.1. Effect of pH on the adsorption capacity

In Fig. 4 it can be observed how the capacity of adsorption of Ni(II) varies at different pH values. The graphs present a sigmoidal behavior.

The maximum adsorption pH is presented at a value of 5.0; At this pH, the predominant species is the Ni(II) ion as seen in Fig. 5. This pH is lower than the pHpcc, so that the mechanism following the Ni(II) adsorption corresponds to the "exchange of protons with the formation of superficial metal complexes ", for hexa-acuo-complexes [M (H$_2$O) 6]$^{n+}$ [23, 60, 61, 62, 63, 64, 65, 66]. This confirms the fact that the pH decreases at the end of the adsorption process, since it releases protons to the medium, as in the exchange of ions, which agrees with the experimental data since at the end of the adsorption process the pH of the Solutions decreases. The experiments of the capacity of adsorption and kinetics are made at pH 5.0.
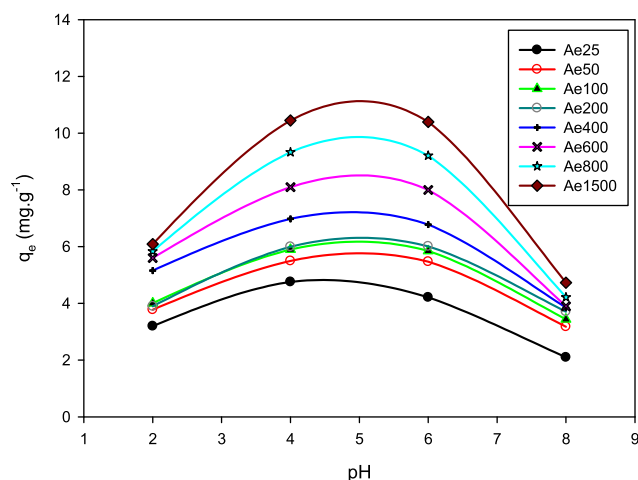


**Fig. 4.** Effect of pH on the capacity of Ni(II) adsorption of carbon aerogels throughout the range of R/C ratios. Co = 100 mg.L$^{-1}$, T = 25 °C. 0.1 g/50 mL. Contact time = 120 minutes.
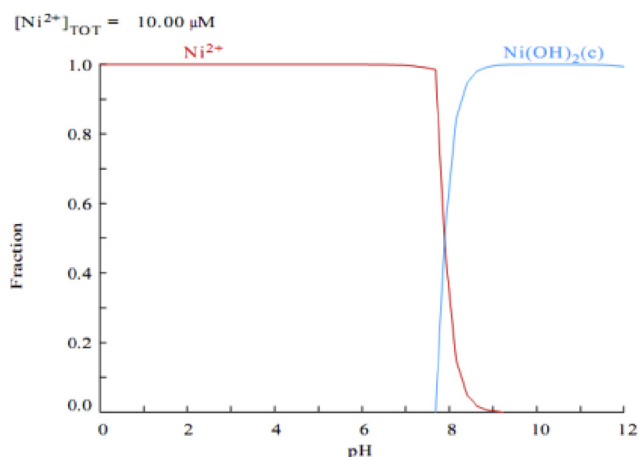
**Fig. 5.** Distribution diagram of nickel species [67].

### 3.4.2. Analysis of the results of the isotherms from aqueous solution for Ni(II)

When analyzing the data obtained when carrying out the adsorption isotherms from aqueous solution, it is observed that increasing the R/C ratio increases the capacity of adsorption as can be seen in Fig. 6. All the isotherms have a more homogeneous and very homogeneous behavior.

similar, without any sample showing any differentiated behavior. At a concentration of 70 and 90 mg.L$^{-1}$, the adsorption begins to reach equilibrium since the plateau that is beginning to become more horizontal is reached and the amount adsorbed no longer increases for high concentrations of Ni(II). The only samples that do not reach a total "plate" are the Ae600, Ae800, and Ae1500, which is probably associated with the fact that these samples could still absorb some more Ni(II).

The adsorption capacities vary from 6.790 mg g$^{-1}$ for sample Ae25, up to 12.55 mg g$^{-1}$ for sample Ae1500. The minimum adsorption value for sample Ae25 is 5.14 mg g$^{-1}$ for carbon aerogels. The maximum value corresponds to the sample Ae1500 and is of 12.55 mg g$^{-1}$ Fig. 7 groups the two series defined as follows: Series-I: Ae25, Ae50, Ae100, Ae200; and Series-II: Ae400, Ae600, Ae800, Ae1500, to continue the same treatment to the analysis.

In both series, there is an increase in the capacity of Ni(II) adsorption as the R/C ratio increases. In the I-series, for the Ae25, Ae50 and Ae100 samples, the capacities are very similar, with a greater difference being observed for the Ae200 sample. This same behavior is observed for the sample Ae1500 with respect to the other three samples of the series-II. As the R/C ratio increases for the two series, the initial part of the isotherms becomes more pronounced, indicating that adsorption is faster for samples with higher R/C, but this can be studied in a better way with the adsorption kinetics.

In Fig. 8 (a-h) the individual isotherms are presented for each sample where the adjustment of the experimental data to the different analysis
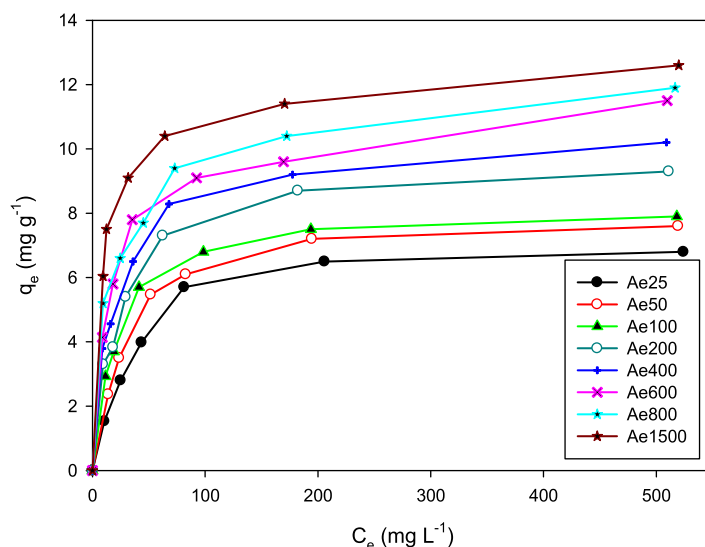


**Fig. 6.** Adsorption isotherms of Ni(II) from aqueous solutions on carbon aerogels throughout the range of R/C ratios.
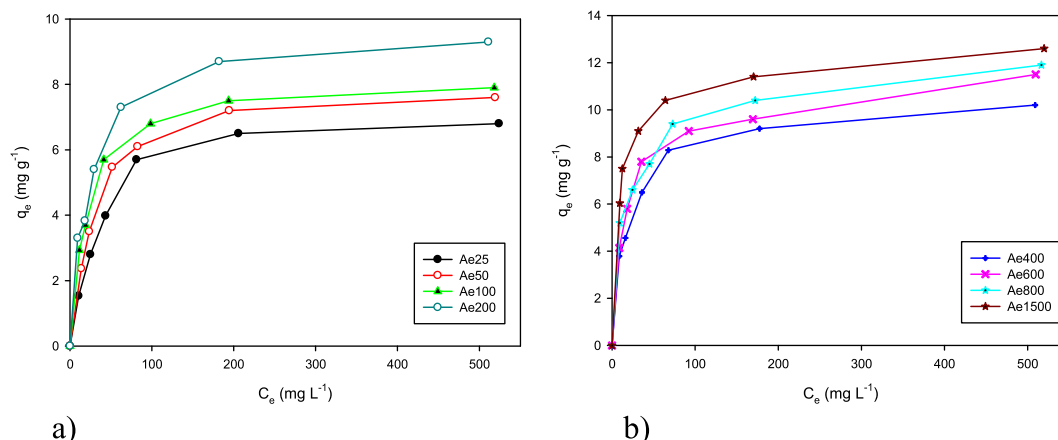


a)



b)

**Fig. 7.** Adsorption isotherms of Ni(II) on carbon aerogels. a) Series-I: Ae25, Ae50, Ae100, Ae200; b) Series-II: Ae400, Ae600, Ae800, Ae1500.
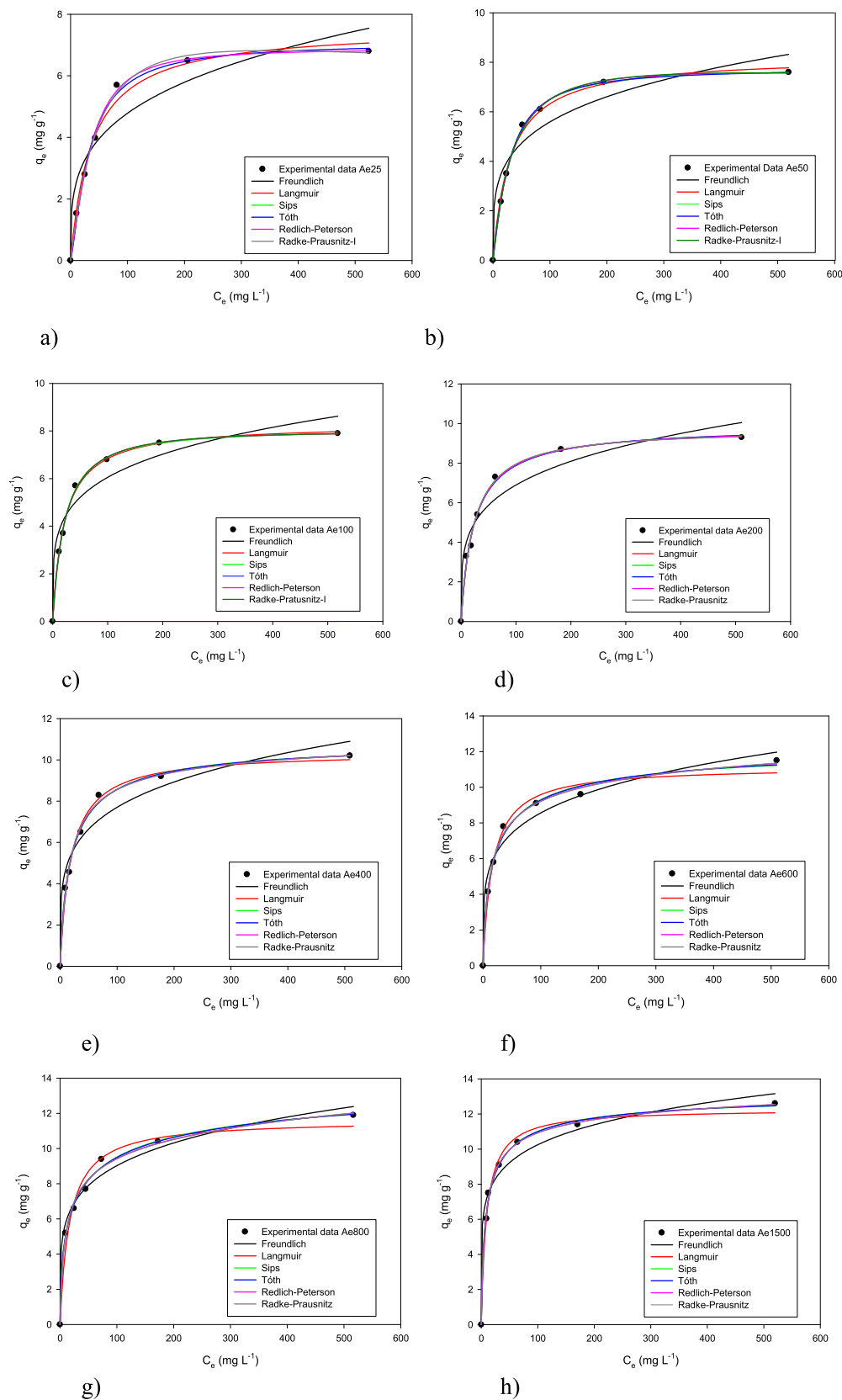
**Fig. 8.** Comparison of experimental data and adsorption isotherms predicted from Ní (II) on carbon aerogels, adjusted to two-parameter models (Freundlich and Langmuir), of three parameters (Sips, Tóth, Redlich-Peterson, and Radke-Prausnitz): a) Ae25, b) Ae50, c) Ae100, d) Ae200, e) Ae400, f) Ae600, g) Ae800 and h) Ae1500.

**Table 4**
Parameters of the Langmuir and Freundlich models for the adsorption of Ni(II) on carbon aerogels throughout the series of R/C.

| Sample | Langmuir | | | Freundlich | | |
|---|---|---|---|---|---|---|
| | $q_m$ (mg $g^{-1}$) | $K_L$ (L $mg^{-1}$) | $R^2$ | $K_f$ ($mg^{1-1/n}$ $L^{1/n}$ $g^{-1}$) | $1/n$ | $R^2$ |
| Ae25 | 7.571 | 0.027 | 0.9894 | 1.348 | 0.275 | 0.9074 |
| Ae50 | 8.220 | 0.033 | 0.9961 | 1.839 | 0.241 | 0.9261 |
| Ae100 | 8.297 | 0.047 | 0.9979 | 2.247 | 0.215 | 0.9407 |
| Ae200 | 9.779 | 0.043 | 0.9927 | 2.379 | 0.231 | 0.9845 |
| Ae400 | 10.38 | 0.053 | 0.9936 | 2.883 | 0.213 | 0.9562 |
| Ae600 | 11.16 | 0.061 | 0.9885 | 3.317 | 0.206 | 0.9710 |
| Ae800 | 11.64 | 0.059 | 0.9771 | 3.717 | 0.193 | 0.9832 |
| Ae1500 | 12.29 | 0.105 | 0.9922 | 5.097 | 0.152 | 0.9760 |

models is illustrated.

According to Fig. 8, the model that presents the lowest adjustment to the experimental data is the Freundlich model, the other two-parameter model that is the Langmuir model presents better adjustments. The three-parameter models used in the present work best describe the adjustments of the experimental data on Ni(II) adsorption on carbon aerogels (see Table 4).

For the two-parameter models, a better fit to the Langmuir model is presented, for all the samples compared to the Freundlich model, even though $R^2$ values are not very good, except for the samples Ae25, Ae600, and Ae800 where the values are the lowest. For the three-parameter models, with respect to the value of $R^2$, the sample that best fits is the Ae50, the other samples have lower values without a specific order, which suggests that the Ni(II) adsorption does not have any correlation with respect to the sites that are available for adsorption.

No definite trend is observed in the behavior of the samples with respect to the models used, establishing the following: Ae50, Ae200, Ae400, and Ae800 adjust with Sips, Ae600 and Ae1500 adjust with Radke-Prausnitz, and Ae25 and Ae100 adjust with Tóth; all samples fit quite well with the three-parameter models (see Table 5). The sample Ae200 presents a very similar adjustment in its values of $R^2$ and this is corroborated in Fig. 8-d, where this behavior is appreciated. The results demonstrate the formation of the monolayer coating of Ni(II) ions on the surface of carbon aerogels. Recalculating the equilibrium adsorption capacity, using the concentration values and the adjustment parameters, we have for Ae25 with the Tóth model, the sample with the lowest adsorption, a value of 6.790 mg $g^{-1}$. For the sample with the highest adsorption with the Radke-Prausnitz Ae1500 model, the amount adsorbed is 9.774 mg $g^{-1}$. Comparing this value with those reported by other authors [67, 68, 69], it can be said that carbon aerogels have a good Ni(II) adsorption capacity from aqueous solution comparable with other adsorbents. Thus, the carbon aerogels obtained in this investigation they are effective for the removal of Ni(II) from aqueous solution at pH = 5.0 and under the experimental conditions used in this study. A preliminary test was carried out on the Ae1500 sample, which is the one with the highest adsorption capacity, with 9.774 mg $g^{-1}$, and it was found that after 4 cycles of use (desorption-adsorption), the capacity of adsorption decreases to 40% in 3.898 mg $g^{-1}$.

*3.4.3. Adsorption kinetics of Ni(II)*

By relating the contact time of the aerogels with the adsorbed amount of Ni(II), a very pronounced initial tendency is observed where the adsorption is very fast in the first minutes, Fig. 9. This indicates that there is a high affinity of the carbon aerogels for the adsorption of Ni(II), upon reaching equilibrium the process becomes slower since the available sites have been occupied by Ni(II) ions and there is a greater impediment for the adsorption to occur.

In the first 15 minutes, very rapid adsorption occurs, where 60% of the amount adsorbed has already been retained by the carbon aerogels. After 60 minutes, the equilibrium begins to be reached, making the adsorption slower. Around 200 minutes the balance is achieved for most
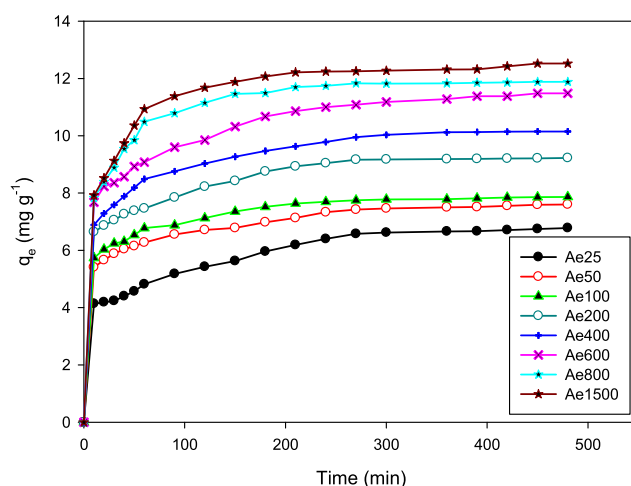


**Fig. 9.** Effect of the contact time with respect to the equilibrium concentrations of experimental Ni(II) data on carbon aerogels. $C_o = 500$ mg.$L^{-1}$, T = 25 °C. 1 g/500 mL. pH = 5.2.

**Table 5**
Parameters of the models of Sips, Tóth, Redlich-Peterson and Radke-Prausnitz, for the adsorption of Ni(II) on carbon aerogels in the entire series of R/C.

| Isotherm | Ae25 | Ae50 | Ae100 | Ae200 | Ae400 | Ae600 | Ae800 | Ae1500 |
|---|---|---|---|---|---|---|---|---|
| **Sips** | | | | | | | | |
| $q_{ms}$ (mg. $g^{-1}$) | 7.082 | 7.805 | 8.123 | 9.916 | 10.91 | 12.40 | 14.53 | 13.26 |
| $K_s$ ($L^m$.$mg^{-m}$) | 0.031 | 0.037 | 0.049 | 0.042 | 0.047 | 0.047 | 0.033 | 0.096 |
| $m_s$ | 1.305 | 1.233 | 1.096 | 0.948 | 0.836 | 0.710 | 0.542 | 0.701 |
| $R^2$ | 0.9954 | 0.9994 | 0.9984 | 0.9929 | 0.9958 | 0.9934 | 0.9957 | 0.9962 |
| **Tòth** | | | | | | | | |
| $q_{mT}$ (mg.$g^{-1}$) | 6.790 | 7.745 | 9.193 | 9.867 | 11.00 | 12.78 | 15.62 | 13.42 |
| $K_T$ | 9.32E-04 | 0.007 | 0.155 | 0.051 | 0.128 | 0.285 | 0.673 | 0.405 |
| $m_T$ | 1.758 | 1.367 | 0.883 | 0.958 | 0.779 | 0.607 | 0.409 | 0.632 |
| $R^2$ | 0.9973 | 0.9993 | 0.9987 | 0.9927 | 0.9955 | 0.9940 | 0.9954 | 0.9964 |
| **Redlich-Peterson** | | | | | | | | |
| $A$ (L.$g^{-1}$) | 0.154 | 0.231 | 0.363 | 0.415 | 0.639 | 0.977 | 1.495 | 1.774 |
| $B$ (L.$mg^{-1}$) | 8.40E-03 | 0.019 | 0.038 | 0.041 | 0.078 | 0.139 | 0.255 | 0.195 |
| $\beta$ | 1.145 | 1.069 | 1.022 | 1.005 | 0.960 | 0.920 | 0.883 | 0.947 |
| $R^2$ | 0.9971 | 0.9988 | 0.9983 | 0.9927 | 0.9951 | 0.9958 | 0.9939 | 0.9971 |
| **Radke-Prausnitz** | | | | | | | | |
| $q_{mRP}$ (mg.$g^{-1}$) | 11.97 | 10.34 | 8.961 | 10.09 | 8.949 | 8.004 | 6.785 | 9.774 |
| $K_{RP}$ (L.$mg^{-1}$) | 1.39E-02 | 0.023 | 0.041 | 0.041 | 0.069 | 0.112 | 0.189 | 0.170 |
| $m_{RP}$ | 1.210 | 1.090 | 1.027 | 1.011 | 0.955 | 0.910 | 0.873 | 0.942 |
| $R^2$ | 0.9966 | 0.9986 | 0.9983 | 0.9927 | 0.9949 | 0.9961 | 0.9935 | 0.9972 |

**Table 6**

Parameters of the kinetic models: pseudo-first-order model - Lagergren, pseudo-second-order model, and intraparticle model - Weber and Morris., For the adsorption of Ni(II) on carbon aerogels in the whole series of R/C.

| Kinetics | Parameters | | Ae25 | Ae50 | Ae100 | Ae200 | Ae400 | Ae600 | Ae800 | Ae1500 |
|---|---|---|---|---|---|---|---|---|---|---|
| | $q_{e\ (expe)}$ | $(mg.g^{-1})$ | 6.789 | 7.612 | 7.887 | 9.314 | 10.19 | 11.49 | 11.89 | 12.55 |
| Pseudo first order | $q_e$ | $(mg.g^{-1})$ | 4.204 | 3.134 | 2.561 | 3.055 | 4.107 | 5.837 | 4.114 | 4.102 |
| | $K_1$ | $(min)^{-1}$ | 0.010 | 0.010 | 0.010 | 0.009 | 0.010 | 0.011 | 0.013 | 0.010 |
| | $R^2$ | | 0.9572 | 0.9491 | 0.9649 | 0.9253 | 0.9742 | 0.9922 | 0.9660 | 0.9119 |
| Pseudo second order | $q_e$ | $(mg.g^{-1})$ | 0.238 | 0.319 | 0.390 | 0.327 | 0.243 | 0.171 | 0.243 | 0.244 |
| | $K_2$ | $(g.mg^{-1}.min^{-1})$ | 0.006 | 0.010 | 0.012 | 0.008 | 0.007 | 0.005 | 0.009 | 0.008 |
| | $R^2$ | | 0.9977 | 0.9992 | 0.9997 | 0.9994 | 0.9995 | 0.9993 | 0.9999 | 0.9999 |
| Intraparticle | $b$ | $(mg.g^{-1})$ | 3.575 | 5.311 | 5.743 | 6.4064 | 6.8924 | 7.470 | 8.3489 | 8.5371 |
| | $K_{ip1}$ | $(mg \cdot g^{-1} \cdot min^{-1/2})$ | 0.162 | 0.1161 | 0.1113 | 0.1483 | 0.170 | 0.2049 | 0.1933 | 0.2129 |
| | $R^2$ | | 0.9586 | 0.9565 | 0.9136 | 0.9290 | 0.9269 | 0.9489 | 0.8057 | 0.7979 |
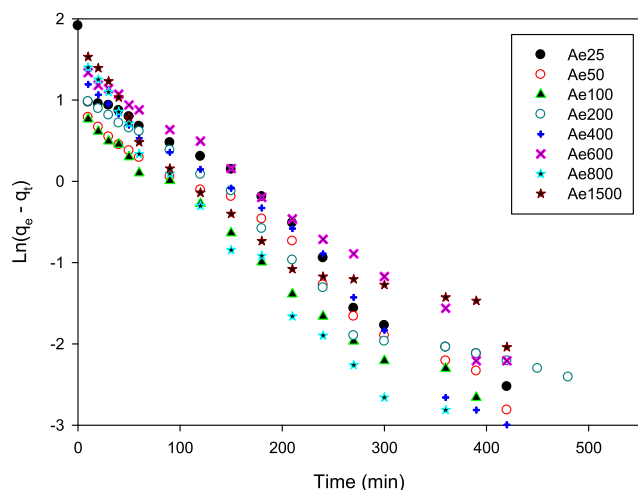


**Fig. 10.** Experimental data adjusted to the pseudo-first order model - Lagergren in the adsorption of Ni(II) on carbon aerogels. $C_o = 500$ mg.L$^{-1}$, T = 25 °C. 1 g/500 mL. pH = 5.0.

samples. Table 6 records the values of the kinetic parameters found for the different models used. The behavior of the kinetics of Ni(II) adsorption on carbon aerogels adjusts in a better way the kinetic model of pseudo-second order since it is the one that presents the value of the highest $R^2$ correlation coefficient. The pseudo-first-order model has lower values of $R^2$, so the kinetics do not fit the experimental data in an adequate way, this is evidenced in Fig. 10 where the dispersion of the data is greater for the whole series of aerogels.
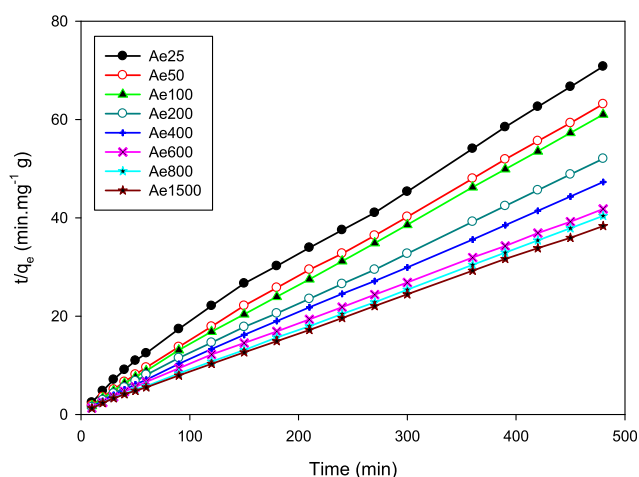
In Fig. 11, the experimental data adjusted to the pseudo-second-order model are observed. The adjustment for the first samples is the lowest of the series, with a slight dispersion of the data and the lower values of $R^2$. The best adjustments are for the latest Ae800 and Ae1500 samples, which have the best $R^2$ value. This is possibly due to the greater development of porosity for higher R/C ratios.

The data adjusted to the Weber and Morris intraparticle model can be seen in Fig. 12. For the first samples, three areas are observed that are not as well defined or marked as if they were observed in the last two samples of the series, Ae800, and Ae1500. This suggests that the first samples present a kinetic where instantaneous adsorption occurs on the external surface, followed by intraparticular diffusion, which is the determining stage of the kinetics, ending with the last stage, which is when the adsorption reaches equilibrium, which is the almost horizontal area of the graphs. For the last two samples, the kinetics is controlled only by the initial instantaneous adsorption, very little intraparticular diffusion and the equilibrium that is achieved.

The intraparticle model presents the lowest values of adjustment with respect to the coefficient of linear regression. These parameters are calculated for a single region of the entire data group since the three zones do not have a well-defined differentiation. Because the graphs do not go through the origin when extrapolating the lines, the difference in the speed of the mass transfer in the initial and final states of the adsorption is different.

### 3.4.4. Results of immersion calorimetry Ni(II)

To correlate the adsorption from aqueous solution of Ni(II) ions and the behavior of carbon aerogels when immersed in such solutions, it is necessary to use special techniques that provide direct information on the
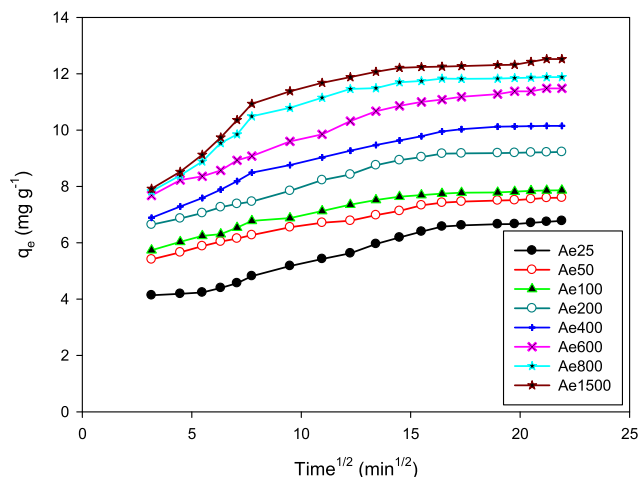


**Fig. 11.** Experimental data adjusted to the pseudo second order model in Ni(II) adsorption on carbon aerogels. Co = 500 mg.L$^{-1}$, T = 25 °C. 1 g/500 mL. pH = 5.0.



**Fig. 12.** Experimental data adjusted to the intraparticle model in Ni(II) adsorption on carbon aerogels. Co = 500 mg.L$^{-1}$, T = 25 °C. 1 g/500 mL. pH = 5,0.
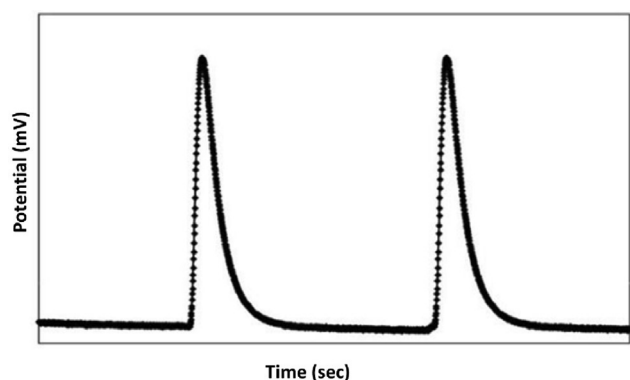
**Fig. 13.** Characteristic thermogram obtained by an isothermal conduction calorimeter.

**Table 7**

Immersion enthalpies for the aerogels carbon series in solutions of Ni(II) 100 mg.L$^{-1}$.

| -Immersion Enthalpy, $\Delta H_{imm}$, (J.g$^{-1}$) | |
| --- | --- |
| Sample | |
| R/C | Ni(II) |
| Ae25 | 70.25 |
| Ae50 | 73.17 |
| Ae100 | 80.13 |
| Ae200 | 84.52 |
| Ae400 | 89.61 |
| Ae600 | 102.5 |
| Ae800 | 108.7 |
| Ae1500 | 110.8 |

particular liquid-solid interactions. Microcalorimetry is a useful and versatile technique for this purpose. The parameter that is evaluated by immersion microcalorimetry is the immersion enthalpy, $\Delta H_{inm}$ [38, 70, 71, 72, 73]. The versatility of immersion calorimetry is because changes in surface area, surface chemistry, or microporosity will result in a change in immersion energy. The calorimeter used is called the microcalorimeter of heat flow, in which thermal conduction is favored by a small thermal resistance which allows the flow of heat between the cell and the surroundings, this flow is detected by sensors that use the seebeck effect [74, 75, 76, 77, 78, 79, 80, 81, 82, 83, 84]. In an immersion calorimeter the heat flow is presented by a small difference of temperature between the surroundings and the cell, product of the immersion of the solid. The magnitude of the temperature difference depends on the amount of heat released per unit of time, the thermal conductivity, the geometry of the cell, the type of sensors and the thermal insulators of the calorimeter. The type of signal obtained by means of the thermopiles is presented in Fig. 13, in this thermogram the conduction of heat to the surroundings is evidenced and it is observed by the descent of the potential signal after the process.

The determination of experimental heat of immersion is determined by the integration of the calorimetric signal, the first signal corresponds to the immersion process, which is basically the rupture of the cell and wetting of the sample. The second signal corresponds to the electric calibration process of the calorimeter. The electrical calibration of the equipment is made by dissipating an electrical work through a resistance of 100 Ω, this calibration allows calculating said electrical work. The calorimeter is allowed to stabilize at room temperature until 20 °C, until the signal at the baseline is between ±2.0 μV for about 30 minutes. Once
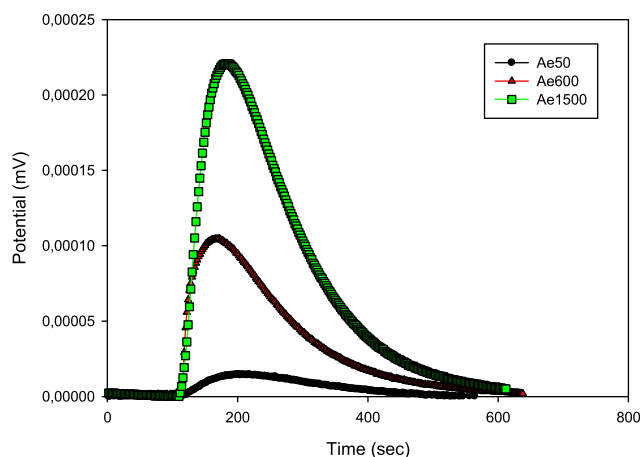
this has been achieved, the immersion is carried out, which is the process of breaking the ampule and later allowing the system to recover the baseline again in a state similar to the initial one. Subsequently, the electrical calibration is performed with a power in such a way that it generates a signal of magnitude similar to the calorimetric signal obtained by the immersion process. The calorimeter constant is 196.6 W.V$^{-1}$, for a dissipated electrical work of approximately 6.0 J, with a sensitivity of $5.0 \times 10^{-3}$ V.W$^{-1}$ and a deviation of less than 2%. The immersion liquids used were prepared from Ni(NO$_3$)$_2$.3H$_2$O in a concentration range of 50 and 500 mg.L$^{-1}$. Fig. 14 shows an example of typical thermograms obtained for 3 aerogels at low, medium and high R/C ratios in a solution of the analyzed ion.

As seen in the thermograms, the effect of the sample with the lowest R/C ratio generates less immersion heat, generating a smooth curve that gradually dissipates towards the end of the process. As the R/C ratio increases, the curve becomes more pronounced, becoming narrower and the generated heat increases more rapidly. When calculating the immersion enthalpy, the degree and nature of the interaction at the solid-liquid interface can be determined, this information is useful since it allows to establish the magnitude of the interactions in the adsorption process. Table 7 shows the values of the immersion enthalpies for the series of carbon aerogels in Ni(II) solutions.

The most negative values correspond to the carbon aerogels for the highest R/C ratios that are also those with the largest surface areas. This shows that in this particular case there is a direct relation between the chemical and textural properties versus the enthalpic value generated in the respective immersion calorimetries.

## 4. Conclusions

During the synthesis process, the aerogels become darker becoming more opaque, the structure becomes more fragile and porous in appearance as the R/C ratio increases, but without losing the monolith structure. In the same way the formation of according to the relation R/C. Aerogels have a high fixed carbon content, this can be seen in the greater development of the carbonaceous structure. This value is between 58.5% and 80.2% for Ae25 and Ae1500 respectively. The ash content for the sample Ae25 is 0.2% which is the lowest value and for the sample, Ae1500 is 0.6%. The percentage of weight loss for the whole series of aerogels is stabilized between 59.4% and 53.8% for Ae25 and Ae1500 respectively. These contents come from the Na$_2$CO$_3$ used as the catalyst of the synthesis, they increase as the R/C ratio. The total acidity for the samples of carbon aerogels is greater than the total basicity. When the carboxylic, lactonic and phenolic groups predominate, the surface of the carbonaceous structure presents good characteristics for the exchange of cationic ions. There are two well-marked trends in the development of porosity as the resorcinol/catalyst ratio increases. In the whole series, an increase in the development of the surface area is observed. All the carbon aerogels prepared in this investigation present an increase in the development of the surface area as the R/C ratio increases, from 64 m$^2$ g$^{-1}$ for the sample Ae25, to 990 m$^2$ g$^{-1}$ for the sample Ae1500. The samples



**Fig. 14.** Thermogram obtained in the immersion of carbon aerogels. Ae50, Ae600 and Ae1500. Ni(II) 100 mg.L$^{-1}$.

obtained are microporous with increasing development of mesoporosity as the R/C ratio increases, being more noticeable in Ae600 and Ae800 samples and a heterogeneous pore distribution.

In the adsorption of Ni(II) on carbon aerogels, the maximum adsorption capacity was given at a pH of 5.0 which is lower than $pH_{pcc}$. It is proposed as an adsorption mechanism "proton exchange with the formation of superficial metal complexes". The adsorption capacity of Ni(II) increases as the R/C ratio increases. When applying the models to determine the capacity of adsorption, those that behave best are the 3-parameter models. This means that the adsorption occurs on a homogeneous surface, which contains sites of equal energy and that are available in the same way for adsorption, improving with the development of porosity as the R/C ratio increases. have more available adsorption sites. The sample of lower adsorption Ae25 with the Tóth model, the value is 6.790 mg g$^{-1}$. The sample with the highest adsorption with the Radke-Prausnitz model Ae1500, the amount adsorbed is 9.774 mg g$^{-1}$. The behavior of the kinetics of Ni(II) adsorption on carbon aerogels adjusts in a better way the kinetic model of pseudo-second order since it is the one that presents the value of the highest $R^2$ correlation coefficient. The results indicate that the prepared carbon aerogels have a great potential for the retention of Ni(II) ions. To the extent that the adsorbed amount is less, the enthalpy is lower. As the surface area increases, the enthalpy of immersion increases.

## Declarations

### Author contribution statement

Rafael Fonseca: Conceived and designed the experiments; Performed the experiments; Analyzed and interpreted the data.

Liliana Giraldo, Juan Carlos Morneo-Piraján: Conceived and designed the experiments; Performed the experiments; Analyzed and interpreted the data; Contributed reagents, materials, analysis tools or data; Wrote the paper.

### Competing interest statement

The authors declare no conflict of interest.

### Additional information

No additional information is available for this paper.

## References

[1] M. Hernández-Rodriguez, J. Yperman, R. Carleerb, J. Maggen, D. Dadi, G. Gryglewicz, B.V. der Bruggen, J.F. Hernández, A. Otero-Calvis, Adsorption of Ni(II) on spent coffee and coffee husk based activated carbon, J. Env. Chem. Eng. 6 (2018) 1161–1170.

[2] Y.F. Jia, B. Xiao, K.M. Thomas, Adsorption of metal ions on nitrogen surface functional groups in activated carbons, Langmuir 18 (2) (2002) 470–478.

[3] T. Aman, A.A. Kazi, M.U. Sabri, Q. Bano, Potato peels as solid waste for the removal of heavy metal copper (II) from waste water/industrial effluent, Colloids Surf., B 63 (2008) 116–121.

[4] K.S. Kasprzak, F.W. Sunderman, K. Salnikow, Nickel carcinogenesis, Mutat. Res. Fund. Mol. M. 533 (2003) 67–97.

[5] Zainab Mahdi, Qiming Jimmy Yu, Ali El Hanandeh, Investigation of the kinetics and mechanisms of nickel and copper ions adsorption from aqueous solutions by date seed derived biochar, J Environ Chem Eng 6 (2018) 1171–1181.

[6] N. Barka, M. Abdennouri, M.E. Makhfouk, S. Qouzal, Biosorption characteristics of cadmium and lead onto eco-friendly dried cactus (Opuntia ficus indica) cladodes, J. Environ. Chem. Eng. 1 (2013) 144.

[7] J. Reungoat, M. Macova, B. Escher, S. Carswell, J. Mueller, J. Keller, Removal of micropollutants and reduction of biological activity in a full scale reclamation plant using ozonation and activated carbon filtration, Water Res. 44 (2010) 625.

[8] E. Dana, A. Sayari, Adsorption of heavy metals on amine-functionalized SBA-15 prepared by co-condensation: applications to real water samples, Desalination 285 (2012) 62.

[9] M. Bilal, T.G. Kazi, H.I. Afridi, M.B. Arain, N. Khan, Application of conventional and modified cloud point extraction for simultaneous enrichment of cadmium, lead and copper in lake water and fish muscles, J. Ind. Eng. Chem. 40 (2016) 137.

[10] M.W. Yap, N.M. Mubarak, J.N. Sahu, E.C. Abdullah, Microwave induced synthesis of magnetic biochar from agricultural biomass for removal of lead and cadmium from wastewater, J. Ind. Eng. Chem. 45 (2017) 287.

[11] C. Gutierrez, H.K. Hansen, P. Hernandez, C. Pinilla, Biosorption of cadmium with brown macroalgae, Chemosphere 138 (2015) 164.

[12] M. Owlad, M.K. Aroua, W.M.A.W. Daud, Hexavalent chromium adsorption on impregnated palm shell activated carbon with polyethyleneimine, Bioresour. Technol. 101 (2010) 5098.

[13] M. El-Sadaawy, O. Abdelwahab, Adsorptive removal of nickel from aqueous solutions by activated carbons from doum seed (Hyphaenethebaica) coat, Alexandria Eng. J. 53 (2014) 399–408.

[14] M. Nadeem, A. Mahmood, S.A. Shahid, S.S. Shah, A.M. Khalid, G. McKay, Sorption of lead from aqueous solution by chemically modified carbon adsorbents, J. Hazard Mater. 138 (2006) 604–613.

[15] F.-S. Zhang, J.O. Nriagu, H. Itoh, Mercury removal from water using activated carbons derived from organic sewage sludge, Water Res. 39 (2005) 389–395.

[16] A.M. Youssef, T. El-Nabarawy, S.E. Samra, Sorption properties of chemically-activated carbons: 1 Sorption of cadmium (II) ions, Colloids Surf. A Physicochem. Eng. Asp. 235 (2004) 153–163.

[17] H. Yanagisawa, Y. Matsumoto, M. Machida, Adsorption of Zn(II) and Cd(II) ions onto magnesium and activated carbon composite in aqueous solution, Appl. Surf. Sci. 256 (2010) 1619–1623.

[18] Ghasemi, M.Z. Khosroshahy, A.B. Abbasabadi, N. Ghasemi, H. Javadian, M. Fattahi, Microwave-assisted functionalization of Rosa Canina-L fruits activated carbon with tetraethylenepentamine and its adsorption behaviour toward Ni(II) in aqueous solution: kinetic, equilibrium and thermodynamic studies, Powder Technol. 274 (2015) 362–371.

[19] F. Fu, Q. Wang, Removal of heavy metal ions from wastewaters: a review, J. Environ. Manag. 92 (2011) 407–418.

[20] R.W. Pekala, Organic aerogel from polycondensation of resorcinol with formaldehyde, J. Mater. Sci. 24 (1989) 3221.

[21] O.P. Mahajan, $CO_2$ surface area of coals: the 25-years paradox", Carbon 29 (1991) 735–741.

[22] H. Treviño-Cordero, L. Juárez, D. Mendoza, V. Hernández, A. Bonilla, M. Montes-Morán, Synthesis and adsorption properties of activated carbons from biomass of Prunus doméstica and Jacaranda mimosifolia for the removal of heavy metals and dyes from water, Ind. Crops Prod. 42 (2013) 315–322.

[23] R.A. Fonseca-Correa, L. Giraldo, J.C. Moreno-Pirajan, Comparison of PSD of carbon aerogels obtained by QSDFT and immersion calorimetry at different resorcinol/catalyst ratio, Microporous Mesoporous Mater. 248 (2017) 164-172.

[24] Rafael Alberto Fonseca-Correa, Marlon Jose Bastidas-Barranco, Liliana Giraldo, Juan Carlos Moreno-Pirajan, Carbon Aerogels: a study with different models of the effect resorcinol/catalyst at different ratios after pyrolysis and the effect on textural properties, Eur. J. Chem. 8 (3) (2017) 279–287.

[25] T.J. Bandosz, Surface chemistry of carbon materials, in: S. Philippe, J.L. Figueiredo (Eds.), Carbon Materials for Catalysis, 2009, pp. 58–59.

[26] H.P. Boehm, Surface oxides on carbon and their analysis: a critical assessment, Carbon 40 (2) (2002) 145–149.

[27] C. Moreno-Castilla, Adsorption of organic molecules from aqueous solutions on carbon materials, Carbon 42 (2004) 83–89.

[28] J.S. Noh, J.A. Schwarz, Estimation of the point of zero charge of simple oxides by mass tritration, J. Colloid Interface Sci. 130 (1989) 157–165.

[29] S. Zalac, N. Kallay, Application of mass titration to the point of zero charge determination, J. Colloid Interface Sci. 149 (1992) 233–239.

[30] W.H. Bragg, in: W.H. Bragg, W.L. y Bragg (Eds.), X-rays and Crystal Structure, Bell & Song, Londres, 1918.

[31] J. Rouquerol, I. Wadso, T.J. Lever, P.J. Haines, Chapter 2. En: Handbook of Thermal Analysis and Calorimetry. Further Advances, Techniques and Applications, Elsevier, Amsterdam, 2007, pp. 13–54.

[32] J. Rouquerol, F. Rouquerol, 3 Methodology of Gas Adsorption. En Adsorption by Powders and Porous Solids Principles, Methodology and Applications, Elsevier Ltd, second ed., Academic Press, Oxford, 2014, pp. 58–87.

[33] J.C. Moreno-Pirajan, L. Giraldo, V. García-Cuello, D. Vargas-Delgadillo, P. Rodríguez-Estupiñán, Y. Murillo-Acevedo, M. Cantillo, Interaction Thermodynamics between Gas-Solid and Solid Liquid on Carbon Materials. En Thermodynamics/Book 1, INTECH, Rijeka, Croatia, 2011, pp. 164–195.

[34] D.P. Vargas, L. Giraldo, J.C. Moreno, Calorimetric study of activated carbons impregnated with CaCl$_2$, Open Chem 13 (2015) 683–688.

[35] L. Giraldo, J.C. Moreno-Pirajan, Calorimetric determination of activated carbons in aqueous solutions, Therm. Anal. Calorim. 89 (2007) 589–594.

[36] R. Luzny, M. Ignaslak, J. Walendzlewskl, M. stolarski, Heavy metals ions removal from aqueous solutions using carbón aerogels and xerogels, Chemik 68 (2014) 544–553.

[37] A.K. Meena, G.K. Mishra, P.K. Rai, Ch. Rajagopal, P.N.R. Nagar, Removal of heavy metal ions from aqueous solutions using carbon aerogel as an adsorbent, J. Hazard Mater. B122 (2005) 161–170.

[38] J. Goel, V. Kadirvelu, C. Rajagopal, V.K. Garg, Cadmium (II) uptake from aqueous solution by adsorption onto carbon aerogel using a response surface methodological approach, Ind. Eng. Chem. Res. 45 (2006) 6531–6537.

[39] J. Goel, K. Kadirvelu, C. Rajagopal, V.K. Garg, Removal of lead(II) from aqueous solution by adsorption on carbon aerogel using a response surface methodological approach, Ind. Eng. Chem. Res. 44 (2005) 1987–1994.

[40] C. Lin, J.A. Ritter, Effect of synthesis pH on the structure of carbon xerogels, Carbon 35 (9) (1997) 1271–1278.

[41] J.P.S. Sousa, M.F.R. Pereira, L.G. Figueiredo, Carbon xerogel catalyst for NO oxidation, Catalysts 2 (2012) 447–465.

[42] J.L. Figueiredo, Carbon xerogels for catalytic applications, Boletin grupo Español del Carbón 12 (2012) 12–17.

[43] P. Rana, N. Mohan, C. Rajagopal, Electrochemical removal of chromium from wastewater by using carbon aerogel electrodes, Water Res. 38 (12) (2004) 2811–2820.

[44] J.C. Farmer, S.M. Bahowick, J.E. Harrar, D.V. Fix, R.E. Martinelli, A.K. Vu, K.L. Carrol, Electrosorption of chromium ions on carbon aerogel electrodes as a means of remediating ground water, Energy Fuels 11 (1997) 337–347.

[45] N.A. Fathy, A.A. Attia, B. Hegazi, Nanostructured activated carbón xerogels for removal of methomyl pesticide, Desalination Water Treat 57 (2015) 1–14.

[46] B.Z. Zapata, G. Diossa, C.D. Castro, G. Quintana, Activated carbon bio-xerogels as electrodes for super capacitors applications, Procedia Eng 148 (2016) 18–24.

[47] H. Maleki, Recent advances in aerogels for environmental remediation applications, Chem. Eng. J. 300 (2016) 98–118.

[48] L.A. Almeida, A. Castro, F. Mendoça, J. Mesquita, Characterization of acid functional groups of carbon dots by nonlinear regression data fitting of potentiometric titration curves, Appl. Surf. Sci. 370 (2016) 486–495.

[49] J. Figueiredo, M.F.R. Pereira, The role of surface chemistry in catalysis with carbons, Catal. Today 150 (2010), 2-1.

[50] H.P. Boehm, Some aspects of the surface chemistry of carbon blacks and other carbons, Carbon 32 (5) (1994) 759–769.

[51] C. Contescu, J. Jagiello, J. Schwarz, Heterogeneity of proton binding sites at the oxide/solution interface, Langmuir 9 (1993) 1754–1765.

[52] A. Dandekar, R.T.K. Baker, M.A. Vannice, Characterization of activated carbon, graphitized carbon fibers and synthetic diamond powder using TPD and DRIFTS, Carbon 36 (1998) 1821–1831.

[53] C.L. Mangun, K.R. Benak, J. Economy, K.L. Foster, Surface chemistry, pore sizes and adsorption properties of activated carbon fibers and precursors treated with ammonia, Carbon 39 (2001) 1809–1820.

[54] P.E. Fanning, M.A. Vannice, A DRIFTS study of the formation of surface groups on carbon by oxidation, Carbon 31 (1993) 721–730.

[55] S. Biniak, G. Szymanski, J. Siedlewski, A. Swiatkowski, The characterization of activated carbons with oxygen and nitrogen surface groups, Carbon 35 (1997) 1799–1810.

[56] D.J. Suh, T.J. Park, S.K. Ihm, Effect of surface oxygen groups of carbon supports on the characteristics of Pd/C catalysts, Carbon 31 (1993) 427–435.

[57] K.S.W. Sing, Assessment of Surface Area by Gas Adsorption. En: Adsorption by Powders and Porous Solids Principles, Methodology and Applications, Elsevier Ltd, second ed., Academic Press, Oxford, 2014, pp. 237–268. Capítulo 7.

[58] K.S.W. Sing, D.H. Everett, R.A.W. Haul, L. Moscou, R.A. Pierotti, J. Rouquerol, T. Siemieniewska, Reporting physisorption data for gas/solid systems with special reference to the determination of surface area and porosity, Pure Appl. Chem. 57 (1985) 603–619.

[59] M. Thommes, K. Kaneko, A.V. Neimark, J.P. Olivier, F. Rodriguez-Reinoso, J. Rouquerol, K.S.W. Sing, Physisorption of gases, with special reference to the evaluation of surface area and pore size distribution (IUPAC Technical Report), Pure Appl. Chem. 87 (2015) 1051–1069.

[60] P.J.M. Carrott, M.M.L. Ribeiro Carrott, Suhas, Comparison of the Dubinin–Radushkevich and Quenched Solid Density Functional Theory approaches for the characterisation of narrow microporosity in activated carbons obtained by chemical activation with KOH or NaOH of Kraft and hydrolytic lignins, Carbon 48 (2010) 4162–4169.

[61] P.I. Ravikovitch, A.V. Neimark, Density functional theory model of adsorption on amorphous and microporous silica materials, Langmuir 22 (2006) 11171–11179.

[62] A.V. Neimark, Y. Lin, P.I. Ravikovitch, M. Thommes, Quenched solid density functional theory and pore size analysis of micro-mesoporous carbons, Carbon 47 (2009) 1617–1628.

[63] J.P. Olivier, Improving the models used for calculating the size distribution of micropore volume of activated carbons from adsorption data, Carbon 36 (1998) 1469–1474.

[64] P.I. Ravikovitch, A. Vishnyakov, R. Russo, A.V. Neimark, Unified approach to pore size characterization of microporous carbonaceous materials from N$_2$, Ar, and CO$_2$ adsorption isotherms, Langmuir 16 (2000) 2311–2319.

[65] A.V. Neimark, P.I. Ravikovitch, A.J. Vishnyakov, Phys: bridging scales from molecular simulations to classical thermodynamics: density functional theory of capillary condensation in nanopores, J. Phys. Condens. Matter 15 (2003) 347-365.

[66] J. Lander, Y.G. Gor, A.V. Neimark, Density functional theory methods for characterization of porous materials, Colloids Surface.: Physicochem. Eng. Aspects 437 (2013) 3–32.

[67] C. Moreno-Castilla, F.J. Maldonado-Hódar, Carbon aerogels for catalysis applications: an overview, Carbon 43 (2005) 455–465.

[68] V. Srivastava, I. Mall, I. Mishra, Competitive adsorption of cadmium (II) and nickel (II) metal ions from aqueous solution onto rice husk ash, Chem.Eng.Pro.: Process Int. 48 (2009) 370–379.

[69] R.W. Pekala, W. Schaefer, Structure of organic aerogels. 1. Morphology and scaling, Macromolecules 26 (1993) 5487–5493.

[70] D. Fairén-Jiménez, F. Carrasco-Marín, C. Moreno-Castilla, Porosity and surface area of monolithic carbon aerogels prepared using alkaline carbonates and organic acids as polymerization catalysts, Carbon 44 (2006) 2301–2307.

[71] C. Moreno-Castilla, M.A. Álvarez-Merino, L.M. Pastrana-Martínez, M.V. López-Ramón, Adsorption mechanisms of metal cations from water on an oxidized carbon Surface, J. Colloid Interface Sci. 345 (2010) 461–466.

[72] Z. Ali, A. Khan, R. Ahmad, The use of functionalized aerogels as a low-level chromium scavenger, Microporous Mesoporous Mater. 203 (2015) 8–16.

[73] O. Hamdaoui, E. Naffrechoux, Modeling of ads. orption isotherms of phenol and chlorophenols onto granular activated carbón Part II. Models with more than two parameters, J. Hazard Mater. 147 (2007) 401–411.

[74] Linhai Pan, Zhuqing Wang, Yang Qi, Rongyi Huang, Efficient removal of lead, copper and cadmium ions from water by a porous calcium alginate/graphene oxide composite aerogel, Nanomaterials 8 (2018) 957.

[75] K.T. Li, G.H. Wu, M. Wang, X.H. Zhou, Z.Q. Wang, Efficient removal of lead ions from water by a low-cost alginate-melamine hybrid sorbent, Appl. Sci. 8 (2018).

[76] N.A. Fathy, O.I. El-Shafey, L.B. Jhalil, Effectiveness of alkali-acid treatment in enhancement the adsorption capacity for rice straw: the removal of methylene blue dye, Phys. Chem. 2013 (2013) 1–15. Hindawi Publishing Corporation.

[77] R. Luzny, M. Ignaslak, J. WalendzleWskl, M. StolaRskl, Heavy metals ions removal from aqueous solutions using carbon aerogels and xerogels, Chemik 68 (2014) 544–553.

[78] Saad A. Al-Jill, Removal of heavy metals from industrial wastewater by adsorption using local bentonite clay and roasted date pits in Saudi arabia, Trends Appl. Sci. Res. 5 (2010) 138–145. ISSN: 1819-3579.

[79] G. Mezohegyi, F. Van der Zee, J. Font, A. Fortuny, A. Fabregat, Towards advanced aqueous dye removal process: a short review on the versatile role of activated carbón, J. Environ. Manag. 102 (2012) 148–164.

[80] F. Rodríguez Reinoso, M. Molina-Sabio, Textural and chemical characterization of microporous carbons, Adv. Colloid Interface Sci. 76 (1998) 271–294.

[81] B. Tansel, P. Nagarajan, SEM study of phenolphthalein adsorption on granular activated Carbon, Adv. Environ. Res. 8 (2004) 411–415.

[82] P. Burg, D. Cagniant, Characterization of Carbon Surface Chemistry En: Chemistry and Physiscs of Carbon, Taylor & Francis Group, New York, 2008, 29-17.

[83] F. Rouquerol, J. Rouquerol, K. Sing, Adsorption by Powder & Porous Solid, Academic Press, London, 1999.

[84] J. Rouquerol, D. Avnir, C.W. Fairbridge, D.H. Everett, J.M. Haynes, N. Pernicone, J.D.F. Ramsay, K.S.W. Sing, K.K. Unger, Recommendations for the characterization of porous solids (Technical Report), Pure Appl. Chem. 66 (1994) 1739.